Nonadiabatic processes in Majorana qubit systems

M. S. Scheurer and A. Shnirman
Institute for Theory of Condensed Matter and DFG Center for Functional Nanostructures (CFN), Karlsruhe Institute of Technology (KIT), Karlsruhe, Germany
(Received 4 June 2013; published 30 August 2013)

We investigate the nonadiabatic processes occurring during the manipulations of Majorana qubits in one-dimensional semiconducting wires with proximity-induced superconductivity. Majorana qubits are usually protected by the excitation gap. Yet, manipulations performed at a finite pace can introduce both decoherence and renormalization effects. Although exponentially small for slow manipulations, these effects are important as they may constitute the ultimate decoherence mechanism. Moreover, as adiabatic topological manipulations fail to produce a universal set of quantum gates, nonadiabatic manipulations might be necessary to perform quantum computation.

DOI: 10.1103/PhysRevB.88.064515 PACS number(s): 03.67.Lx, 73.63.Nm, 03.67.Pp, 71.10.Pm

I. INTRODUCTION

Various realizations of zero-energy Majorana bound states (MBS) are currently being intensively investigated.[1] Initially introduced in rather abstract models,[2–4] they started to look realistic after several heterostructures that might host such modes were proposed.[5–7] In all these heterostructures, superconductivity is proximity induced into a semiconductor with strong spin-orbit coupling[6,7] or into a surface state of a topological insulator.[5]

Two MBS form a regular (Dirac) fermion which can be either occupied or nonoccupied. These states are of different fermion parity and, thus, can not be used as a qubit. However, setups with more MBS, e.g., two pairs of Majorana modes, are already rich enough to encode qubits within the subspace of a given parity. Topological manipulations of these qubits require "braiding" of MBS. In the simplest realization, one just "mechanically" moves one MBS around another. This can be achieved by applying time-dependent gates.[8] More sophisticated braiding schemes have been suggested (see, e.g., Refs. 9 and 10).

In this paper, we study the nonadiabatic effects occurring when the MBS are "mechanically" shifted. Yet, the formalism introduced here is rather general and can be applied in more involved setups. Decoherence effects in Majorana qubits have already been addressed.[11–16] Coupling to a gapless fermonic bath is definitely detrimental.[11] In Refs. 12–14, a general framework of decoherence in situations when the gap is preserved was introduced. In contrast to Refs. 12–14, we perform the adiabatic perturbation expansion for a concrete physical system calculating the nonadiabatic coupling matrix (Berry matrix) explicitly. For the proximity-coupled nanowire setup considered in this work, only numerical studies of the dynamical formation of Majorana modes[15] exist and decoherence caused by fluctuating gates[16] has been studied.

We distinguish two major effects. First, due to the motion of the MBS, a quasiparticle in the continuum may be excited, somewhat analogously to the Landau-Zener tunneling. The probability of such an event is exponentially small, unless the velocity of the MBS approaches a certain critical velocity. Such a process changes the parity of the qubit subspace, thus giving rise to decoherence. Second, the coupling between two remote Majorana modes can get renormalized if both MBS are moved simultaneously. This coupling lifts the degeneracy between the empty and the occupied states of the corresponding Dirac fermion. On the one hand, this renormalization effect has, thus, to be accounted for, if we aim at performing quantum gates with high accuracy. On the other hand, it may be generated intentionally in order to induce nontopological phase gates.

This paper is organized as follows: In Sec. II, we first present the formalism that is used in this work for treating nonadiabatic effects and investigate a general time-dependent topological superconductor of class BDI, D, or DIII. Furthermore, an effective Hamiltonian for the qubit incorporating nonadiabatic corrections is derived. Then, we focus on the quantum wire proposal and discuss both the limitations arising from the presence of the states above the gap of the system (see Sec. III) as well as the possibility of creating a phase gate that is based on nonadiabatic effects (see Sec. IV).

II. GENERAL EXPRESSIONS FOR NONADIABATIC PROCESSES

In this section, nonadiabatic processes in systems hosting MBS are analyzed from a generic point of view, i.e., without referring to any of the specific realizations of Majorana modes in condensed matter systems.

A. Formalism

Although a similar treatment of time-dependent Bogoliubov–de Gennes (BdG) equations has already been used in the context of Majorana fermions,[13] we present our own formulation best suited for the analysis in this paper. Let us begin with the general time-dependent BCS mean-field Hamiltonian

$$\hat{\mathcal{H}}(t) = \frac{1}{2}\int d\vec{r}\int d\vec{r}\,'\,\hat{\Psi}^{\dagger}(\vec{r})h(t)\hat{\Psi}(\vec{r}\,') \tag{1}$$

written in the standard quadratic BdG form. For simplicity, spinor indices have been skipped. The field operators $\hat{\Psi}(\vec{r})$ are Nambu spinors satisfying the Majorana condition,

$$C_{j,k}\hat{\Psi}_k^{\dagger}(\vec{r}) = \hat{\Psi}_j(\vec{r}), \tag{2}$$

where C is the (unitary) spinor part of the (antiunitary) charge conjugation operator $\Xi = C\mathcal{K}$ with $\mathcal{K}$ denoting complex

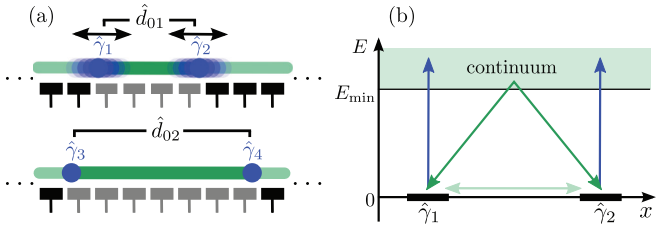

FIG. 1. (Color online) (a) One example for the origin of the time dependence of the BdG Hamiltonian in Eq. (1). The position of the Majorana modes is modified via a "keyboard" of gates as suggested in Ref. 8. Here, the situation is shown where only the MBS belonging to the fermion $\hat{d}_{01}$ are in motion. This is the setup we will focus on in Secs. III and IV. (b) Illustration of adiabatic (light green arrow) and nonadiabatic (dark green) MBS-MBS as well as MBS-continuum (blue) processes.

conjugation. Throughout this paper, we assume that $\Xi^2 = +\mathbb{1}$. Since, in addition, the system may or may not be invariant under time reversal Θ, the analysis of this section applies to superconductors of class[17] D (no time-reversal symmetry), DIII ($\Theta^2 = -\mathbb{1}$), and BDI ($\Theta^2 = \mathbb{1}$). In Secs. III and IV, we will consider an example of a superconductor of class BDI.

Due to its internal redundancy, $\hat{\Psi}(\vec{r})$ satisfies the Majorana anticommutation relations

$$\{\hat{\Psi}_j(\vec{r}),\hat{\Psi}_k(\vec{r}\,')\} = C_{j,k}\delta(\vec{r}-\vec{r}\,'), \tag{3a}$$

$$\{\hat{\Psi}_j(\vec{r}),\hat{\Psi}_k^\dagger(\vec{r}\,')\} = \delta_{j,k}\delta(\vec{r}-\vec{r}\,'), \tag{3b}$$

as opposed to those of ordinary fermions. Additionally, charge conjugation symmetry imposes the constraint $\{h(t),\Xi\} = 0$ making the instantaneous spectrum symmetric about zero energy.

Note that the ansatz (1) only allows for the coupling of the system to a classical field. Apart from that, the time dependence of $\hat{\mathcal{H}}(t)$ is not further specified throughout this section. To be concrete, one may imagine that vortices of a two-dimensional $p_x + ip_y$ superconductor[4] or domain walls in a quantum wire are manipulated, e.g., by the local tuning of external gates[8] as illustrated in Fig. 1(a). Eventually, the results of this section can be applied to any system supporting MBS (see, e.g., Refs. 18–21).

Let us introduce the instantaneous eigenstates $|\phi_n(t)\rangle$ of the BdG Hamiltonian satisfying

$$h(t)|\phi_n(t)\rangle = E_n(t)|\phi_n(t)\rangle, \tag{4}$$

which are chosen to be continuous as a function of t. To fix the relative phase of the instantaneous eigenstates at different times, we impose the parallel transport condition

$$\langle\phi_n(t)|\partial_t\phi_n(t)\rangle = 0. \tag{5}$$

This allows us to define the corresponding instantaneous BdG operators

$$\hat{d}_n(t) := \int d\vec{r}\,\phi_n^\dagger(\vec{r},t)\hat{\Psi}(\vec{r}). \tag{6}$$

Both the field operators $\hat{\Psi}(\vec{r})$ and the eigenfunctions $\phi_n(\vec{r},t)$ have spinor structure and hence summation over spinor components is implied. Physically, these operators correspond to the annihilation of a particle in one of the instantaneous eigenstates at a given time t. They constitute the central objects of our analysis since all physical quantities to be calculated in the following can be written in terms of $\hat{d}_n(t)$ and $\hat{d}_n^\dagger(t)$. It is straightforward to show that $\hat{d}_n^\dagger(t) = \hat{d}_{\bar{n}}(t)$ and

$$\{\hat{d}_n(t),\hat{d}_m(t)\} = \delta_{n,\bar{m}}, \quad \{\hat{d}_n(t),\hat{d}_m^\dagger(t)\} = \delta_{n,m}, \tag{7}$$

where $\bar{n}$ is a shorthand notation for the charge conjugate of state n ($E_{\bar{n}} = -E_n$).

Suppose that diagonalizing $h(t)$ yields M pairs of quasi-zero-energy subgap states $\{|\phi_{0j}(t)\rangle,|\phi_{\overline{0j}}(t)\rangle\}$ with $j = 1,2,\ldots,M$. Denoting the corresponding BdG operators by $\hat{d}_{0j}(t)$, we can define $2M$ time-dependent MBS operators

$$\hat{\gamma}_{2j-1}(t) := \frac{1}{\sqrt{2}}(\hat{d}_{0j}(t) + \hat{d}_{0j}^\dagger(t)), \tag{8a}$$

$$\hat{\gamma}_{2j}(t) := \frac{1}{\sqrt{2}i}(\hat{d}_{0j}(t) - \hat{d}_{0j}^\dagger(t)), \tag{8b}$$

which satisfy by construction

$$\hat{\gamma}_j^\dagger(t) = \hat{\gamma}_j(t) \quad \text{and} \quad \{\hat{\gamma}_i(t),\hat{\gamma}_j(t)\} = \delta_{i,j}. \tag{9}$$

The energies E_{0j} typically scale exponentially with the distance between different MBS (see, e.g., Refs. 22 and 23). Equation (8) makes clear that a Majorana mode is, in contrast to the ordinary fermions $\hat{d}_n$, generally[24] not an exact eigenstate of the Hamiltonian of a finite system. We emphasize that for $M > 1$ one is left with the additional task of finding the correct superpositions of the $\hat{\gamma}_i$ such that the associated Majorana wave functions are spatially localized. However, for $M = 1$, Eq. (8) is already sufficient. Note that the parallel transport condition (5) is automatically satisfied by the wave functions $|\phi_{\gamma_j}\rangle$ of the MBS due to the self-conjugate property $\Xi|\phi_{\gamma_j}\rangle = |\phi_{\gamma_j}\rangle$.

Using the anticommutation relations (7), it is easy to show that the Heisenberg equations of motion for the instantaneous BdG operators read as

$$i\frac{d}{dt}\hat{d}_n^H(t) = \sum_m h'_{n,m}(t)\hat{d}_m^H(t), \tag{10}$$

where

$$\hat{d}^H(t) = \hat{\mathcal{U}}^\dagger(t)\hat{d}_n(t)\hat{\mathcal{U}}(t), \quad \hat{\mathcal{U}}(t) = \mathcal{T}e^{-i\int_{t_0}^t dt'\hat{\mathcal{H}}(t')} \tag{11}$$

are the instantaneous BdG operators in the Heisenberg picture and

$$h'_{n,m}(t) = E_n(t)\delta_{n,m} - \mathcal{M}_{n,m}(t) \tag{12}$$

with $\mathcal{M}_{n,m}(t) = i\langle\phi_n(t)|\partial_t\phi_m(t)\rangle$ has been introduced. The summation in Eq. (10) includes all instantaneous eigenstates with both positive and negative energies. Note that h' is the "moving frame" Hamiltonian of h, which is well known[25] from the study of nonadiabatic quantum mechanics. Nonvanishing values of $\mathcal{M}_{n,m}$ are due to the time dependence of the basis states in Eq. (6). For the particularly important case of $n = 0j$ and m referring to a state above the gap (as well as $n \leftrightarrow m$), these matrix elements give rise to transitions from the ground-state manifold, i.e., the topological qubit(s), to excited

states. These kinds of nonadiabatic processes represent the major focus of our analysis.

The formal solution of the Heisenberg equation (10) is given by

$$\hat{d}_n^H(t) = \sum_m u_{n,m}(t)\hat{d}_m(t_0), \tag{13}$$

where the time-ordered matrix exponential

$$u_{n,m}(t) := \left[\mathcal{T}\exp\left(-i\int_{t_0}^{t} dt'\, h'(t')\right)\right]_{n,m} \tag{14}$$

has been defined. In the following, we will use Eq. (13) to express the nonadiabatic time evolution of a topological qubit in terms of the matrix elements $u_{n,m}(t)$.

B. Qubit quantities

For the remainder of this paper, the analysis is restricted to a single logical qubit, i.e., four[26] Majorana modes $\gamma_1,\ldots,\gamma_4$, which we pair into ordinary fermions according to

$$\hat{d}_{01}(t) = \frac{1}{\sqrt{2}}(\hat{\gamma}_1(t) + i\hat{\gamma}_2(t)), \tag{15a}$$

$$\hat{d}_{02}(t) = \frac{1}{\sqrt{2}}(\hat{\gamma}_3(t) + i\hat{\gamma}_4(t)). \tag{15b}$$

Further MBS may be present in the sample, but are assumed to be inert and sufficiently far away to be safely neglected. The many-body ground-state wave functions are defined as usual,

$$|n_1\, n_2\,(t)\rangle := (\hat{d}_{01}^\dagger(t))^{n_1}(\hat{d}_{02}^\dagger(t))^{n_2}|00(t)\rangle, \tag{16}$$

where $|00(t)\rangle$ denotes the vacuum of the fermions $\hat{d}_{0j}(t)$, $j = 1,2$. Note that, in the present case, the operators and hence the states are time dependent. Without loss of generality, we take the even fermion parity sector $\{|00(t)\rangle, |11(t)\rangle\}$ to form the logical basis of the qubit and assume that it was at the initial time t_0 prepared in a pure state within this subspace. In addition, the initial density matrix $\hat{\rho}(t_0)$ is taken to be diagonal in the occupation number basis with respect to the fermions $\hat{d}_n$ of the continuum.

For simplicity, let us assume that the MBS γ_3, γ_4 are both spatially fixed, decoupled from γ_1, γ_2 and from each other. Thus, their role is reduced to providing the proper Hilbert space for the qubit. This means

$$u_{\gamma_k,n}(t) = \delta_{\gamma_k,n} \tag{17}$$

for $k = 3,4$ [see Fig. 1(a) for an illustration in the system of locally gated nanowires]. Since only the Majorana modes γ_1 and γ_2 belonging to one and the same fermion contribute to transitions, this situation will be referred to as "intrafermionic motion" in the following. The analysis is readily generalized to the situation, where all four MBS are moving simultaneously, however, the results do not convey additional physical insights.

1. Single-fermion parity

The first quantity we use to describe the dynamics of the topological qubit is the parity of the Dirac fermion d_{01} built from γ_1 and γ_2, which is defined by

$$\hat{\mathcal{P}}_{01}(t) := \mathbb{1} - 2\hat{d}_{01}^\dagger(t)\hat{d}_{01}(t) = 2i\hat{\gamma}_2(t)\hat{\gamma}_1(t). \tag{18}$$

The fermion parity constitutes a frequently used[12,13] observable to describe the fidelity of the topological memory. We emphasize that, regarding the qubit, a change in the expectation value of $\hat{\mathcal{P}}_{01}(t)$ can in general be due to two distinct processes, namely, $|00\rangle \leftrightarrow |10\rangle$ (leaving the subspace of the logical two-level system and exciting a quasiparticle in the continuum) and $|00\rangle \leftrightarrow |11\rangle$ (bit-flip error within the logical subspace). In the present case of intrafermionic motion (uncoupled γ_3 and γ_4), only errors of the former type can occur.

Using Eq. (13), $\hat{d}_n^\dagger = \hat{d}_{\bar{n}}$ and $u_{\bar{n},\bar{m}} = u_{n,m}^*$ due to charge conjugation symmetry as well as the unitarity of u, one can write

$$\begin{aligned}\langle\hat{\mathcal{P}}_{01}(t)\rangle_t = \langle\hat{\mathcal{P}}_{01}(t_0)\rangle_{t_0}\left[u_{\gamma_1,\gamma_1}(t)u_{\gamma_2,\gamma_2}(t) - u_{\gamma_1,\gamma_2}(t)u_{\gamma_2,\gamma_1}(t)\right] \\ + 2\sum_{n>0}\langle\hat{\mathcal{P}}_n(t_0)\rangle_{t_0}\mathrm{Im}\left[u_{\gamma_2,n}^*(t)\,u_{\gamma_1,n}(t)\right].\end{aligned} \tag{19}$$

Here, the notation $n > 0$ indicates that the summation is restricted to positive-energy eigenstates of the continuum.

To restate this result in a more explicit form, we now apply time-dependent perturbation theory treating the coupling matrix $\mathcal{M}$ in Eq. (12) as the perturbation. For the moment, let us additionally assume that γ_1 and γ_2 are sufficiently separated such that the energy splitting E_{01} and the ground-state Berry phases can be neglected. Then, second-order perturbation theory yields

$$\begin{aligned}\langle\hat{\mathcal{P}}_{01}(t)\rangle_t = \langle\hat{\mathcal{P}}_{01}(t_0)\rangle_{t_0}\left(1 - \sum_{j=1,2}\sum_{n>0}\left|\int_{t_0}^{t} dt'\mathcal{M}_{\gamma_j,n}(t')e^{-i\int_{t_0}^{t'}dt_1 E_n(t_1)}\right|^2\right) \\ + 2\sum_{n>0}\langle\hat{\mathcal{P}}_n(t_0)\rangle_{t_0}\mathrm{Im}\left[\left(\int_{t_0}^{t} dt'\mathcal{M}_{\gamma_1,n}(t')e^{-i\int_{t_0}^{t'}dt_1 E_n(t_1)}\right)\times(\gamma_1\to\gamma_2)^*\right] + \mathcal{O}(\mathcal{M}^3).\end{aligned} \tag{20}$$

In the first line, the negative-energy eigenstates have been replaced by means of the relation $\mathcal{M}_{\bar{n},\bar{m}} = -\mathcal{M}_{n,m}^*$.

As schematically shown in Fig. 1(b), one can in principle distinguish between two types of processes contributing to the time evolution of the topological qubit. The MBS can either couple locally to the continuum states (blue arrows) or communicate with each other. The latter type of processes contains both direct MBS-MBS tunneling (light green arrows) and nonadiabatic corrections involving virtual states in the continuum as indicated by the dark green arrows.

In the results presented above for the single-fermion parity, we can identify both contributions. The first term in the first line of Eq. (19) and the first line of Eq. (20) are (to leading order) local, whereas all remaining contributions are purely nonlocal and describe correlation effects between different MBS. Note that, when neglecting the nonlocal terms, the result (20) for the fermion parity reduces to the expression obtained in Ref. 12.

2. *Off-diagonal component of the density matrix*

For a more refined picture of the time evolution of the qubit, let us investigate the off-diagonal matrix element of its reduced density matrix, i.e.,

$$\rho_{01}^{Q}(t) := \langle 00(t)|\hat{\rho}^{Q}(t)|11(t)\rangle = \langle \hat{d}_{01}^{\dagger}(t)\hat{d}_{02}^{\dagger}(t)\rangle_{t} \tag{21}$$

with $\hat{\rho}^{Q}(t) = \mathrm{Tr}_{C}\,[\hat{\rho}(t)]$, where $\mathrm{Tr}_{C}\,[\ldots]$ stands for the partial trace taken over the continuum states above the gap. We emphasize that $\rho_{01}^{Q}(t)$ is relevant for two reasons: First, the reduction of its magnitude describes decoherence. Note that, in the case of intrafermionic motion, the main decoherence mechanism is leaving the logical Hilbert space of the qubit. Second, the change of the phase of $\rho_{01}^{Q}(t)$ means that a phase gate can be performed by mutual motion of the two MBS. Generating a time-dependent phase of $\rho_{01}^{Q}(t)$ by nonadiabatic effects may provide alternative routes for implementing phase gates, which are crucial[27] for realizing universal quantum computation (see Sec. IV).

Due to the assumption of intrafermionic motion, we have $u_{\overline{02},n} = \delta_{\overline{02},n}$ and the calculation becomes particularly straightforward:

$$\rho_{01}^{Q}(t) = \sum_{n} u_{\overline{01},n}(t)\langle \hat{d}_{n}(t_0)\hat{d}_{02}^{\dagger}(t_0)\rangle_{t_0} \tag{22}$$

$$= \rho_{01}^{Q}(t_0) \times u_{\overline{01},\overline{01}}(t,t_0). \tag{23}$$

Despite its simplicity, it is instructive to restate Eq. (23) in the Majorana basis in the form

$$\rho_{01}^{Q}(t) = \rho_{01}^{Q}(t_0) \times [c(t) + i\,s(t)] \tag{24}$$

with the real-valued[28] functions

$$c(t) = \tfrac{1}{2}\big[u_{\gamma_1,\gamma_1}(t) + u_{\gamma_2,\gamma_2}(t)\big], \tag{25a}$$

$$s(t) = \tfrac{1}{2}\big[u_{\gamma_1,\gamma_2}(t) - u_{\gamma_2,\gamma_1}(t)\big]. \tag{25b}$$

This result reveals that nonvanishing matrix elements u_{γ_j,γ_k} with $j \neq k$ in Eq. (25b), i.e., nonlocal processes, are required to have $s(t) \neq 0$ and are thus essential for generating a time-dependent phase of $\rho_{01}^{Q}(t)$. Without these processes, the system can only experience decoherence due to the local terms in Eq. (25a).

Again assuming well-separated MBS, one finds within second-order perturbation theory in $\mathcal{M}$

$$\rho_{01}^{Q}(t) = \rho_{01}^{Q}(t_0) \times \exp[\Gamma(t) + i\varphi(t)] + \mathcal{O}(\mathcal{M}^3), \tag{26}$$

where the decoherence function and the accumulated phase are given by

$$\Gamma(t) = -\frac{1}{2}\sum_{j=1,2}\sum_{n>0}\left|\int_{t_0}^{t} dt'\,\mathcal{M}_{\gamma_j,n}(t')e^{-i\int_{t_0}^{t'} dt_1 E_n(t_1)}\right|^2 \tag{27a}$$

and

$$\varphi(t) = \sum_{n>0}\left(\int_{t_0}^{t} dt' \int_{t_0}^{t'} dt''\,\mathrm{Re}\big[\mathcal{M}_{\gamma_2,n}(t')\mathcal{M}^{*}_{\gamma_1,n}(t'')e^{-i\int_{t''}^{t'} dt_1 E_n(t_1)}\big] - (\gamma_1 \leftrightarrow \gamma_2)\right), \tag{27b}$$

respectively. As anticipated by the exact expression (25), the leading contribution to the decoherence is only due to the local coupling of each of the MBS to the continuum and thus solely depends on the motions of the Majorana modes separately. On the contrary, the phase $\varphi(t)$ generated by the process crucially depends on the correlation of the motions of the spatially separated Majorana modes and can only be present if the coupling of both MBS to the continuum is nonzero. As expected, the change of the fermion parity (leaving the logical Hilbert space of the qubit) in Eq. (20) is directly related to the decoherence function (27a), if only one of the Majorana modes is in motion.

C. Effective theory for nearly adiabatic manipulation

In this section, an effective Hamiltonian governing the dynamics within the ground-state manifold is derived. Since nonadiabatic effects are treated in a perturbative manner, its validity is limited to the regime of nearly adiabatic processes. Here, we consider the general case of $2M$ Majorana modes and account for finite overlaps between different localized states.

To integrate out the continuum states, a method taken from Refs. 29 and 30 is applied which we generalize to the case of time-dependent energies $E_n(t)$. The basic idea is to find an effective Hamiltonian $h_{\mathrm{eff}}(t)$ that reproduces the exact time-evolution operator of $h'(t)$ in Eq. (12) within the ground-state subspace. In the interaction picture (again taking $h_1' = -\mathcal{M}$ as perturbation), we demand that

$$P_0\,\mathcal{T}e^{-i\int_{t_0}^{t} dt'\,\tilde{h}_1'(t')}P_0 \overset{!}{=} \mathcal{T}e^{-i\int_{t_0}^{t} dt'\,\tilde{h}_{\mathrm{eff},1}(t')}, \tag{28}$$

where $P_0 := \sum_{\sigma}|\phi_\sigma\rangle\langle\phi_\sigma|$ is the projection operator onto the ground-state manifold. In Fig. 2, a graphical representation of the expansion of both sides of Eq. (28) and of the resulting effective interaction Hamiltonian $\tilde{h}_{\mathrm{eff},1}$ within second order in $\mathcal{M}$ is shown. Since the second-order contribution in the last line of Fig. 2 has two time arguments, further approximations are required to obtain an effective Hamiltonian which is local

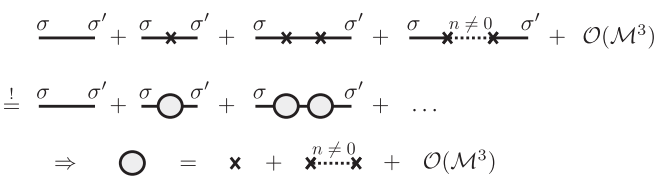

FIG. 2. Schematic illustration of the procedure for determining the effective ground-state Hamiltonian according to Eq. (28). Excited states (dashed lines) are absorbed into an effective ground-state vertex (circle). For slowly varying energies and coupling matrix elements (crosses) the result in the last line is approximately local in time (see main text).

in time. For this purpose, let us assume that both all coupling matrix elements $\mathcal{M}_{\sigma,n}$ and the instantaneous energies E_n vary slowly on the scale set by the gap $E_{\min}$ of the system or more formally

$$\frac{\partial_t E_n(t)}{E_{\min}^2} \ll 1, \quad \frac{1}{E_{\min}} \frac{\partial_t B_{\sigma,n}(t)}{B_{\sigma,n}(t)} \ll 1. \tag{29}$$

An expansion up to first order in these small quantities finally yields

$$\begin{aligned}[h_{\text{eff}}(t)]_{\sigma,\sigma'} \simeq\ & E_\sigma \delta_{\sigma,\sigma'} - \mathcal{M}_{\sigma,\sigma'} \\ & - \sum_{n\neq 0} \left[\frac{\mathcal{M}_{\sigma,n}\mathcal{M}^*_{\sigma',n}}{E_n - \overline{E}_{\sigma,\sigma'}} \left(1 - \frac{i\partial_t (E_\sigma - E_{\sigma'})}{4(E_n - \overline{E}_{\sigma,\sigma'})^2}\right) \right. \\ & \left. - i \frac{\dot{\mathcal{M}}_{\sigma,n}\mathcal{M}^*_{\sigma',n} - \mathcal{M}_{\sigma,n}\dot{\mathcal{M}}^*_{\sigma',n}}{2(E_n - \overline{E}_{\sigma,\sigma'})^2} \right], \end{aligned} \tag{30}$$

upon introducing $\overline{E}_{\sigma,\sigma'} := (E_\sigma + E_{\sigma'})/2$. Here, the explicit time dependence of the matrix elements and of the energies has been omitted for notational convenience. The first-order contributions [first line in Eq. (30)] are simply given by the projection of $h'(t)$ onto the ground-state manifold and thus describe adiabatic processes only. The second-order terms (second and third line), however, constitute nonadiabatic corrections incorporating high-energy degrees of freedom above the gap in the form of single virtual states. Note that the effective Hamiltonian is Hermitian within the present approximations and hence the total parity of the ground-state subspace is conserved. Interestingly, the last line in Eq. (30) is a sum of terms of the form $i(x\dot{y} - \dot{x}y)/2$, upon choosing $x = \mathcal{M}^*_{\sigma',n}/(E_n - \overline{E}_{\sigma,\sigma'})$ and $y = \mathcal{M}_{\sigma,n}/(E_n - \overline{E}_{\sigma,\sigma'})$. Since $x, y \to 0$ for $|t| \to \infty$, the time integral $\int_{-\infty}^{\infty} dt\, (x\dot{y} - \dot{x}y)/2$ is given by the area enclosed by the trajectory $(x(t), y(t))$. Consequently, the leading contribution of this term to the time evolution has a purely geometric interpretation.

For future reference, let us investigate the simplest case with only two MBS ($M = 1$). Taking the particle-hole symmetry of h_{eff} into account, we know that $(h_{\text{eff}})_{\bar{\sigma},\sigma} = -(h_{\text{eff}})^*_{\sigma,\bar{\sigma}} = -(h_{\text{eff}})_{\bar{\sigma},\sigma} = 0$. Therefore, the presence of the excited states only leads to a renormalization of the energy splitting of the MBS, i.e., the effective Hamiltonian written in the basis $\{|\phi_\sigma\rangle, |\phi_{\bar{\sigma}}\rangle\}$ assumes the simple form

$$h_{\text{eff}}(t) \simeq [E_{01}(t) + \delta E(t)]\tau_z, \tag{31}$$

where the energy correction is given by

$$\delta E(t) = -\sum_{n\neq 0} \left[\frac{|\mathcal{M}_{01,n}|^2}{E_n - E_{01}} - i \frac{\dot{\mathcal{M}}_{01,n}\mathcal{M}^*_{01,n} - \mathcal{M}_{01,n}\dot{\mathcal{M}}^*_{01,n}}{2(E_n - E_{01})^2} \right] \tag{32}$$

$$\simeq \sum_{n>0} \left[\frac{2\,\text{Im}\left[\mathcal{M}^*_{\gamma_1,n}\mathcal{M}_{\gamma_2,n}\right]}{E_n} + \frac{\text{Re}\left[\dot{\mathcal{M}}^*_{\gamma_1,n}\mathcal{M}_{\gamma_2,n} - \mathcal{M}^*_{\gamma_1,n}\dot{\mathcal{M}}_{\gamma_2,n}\right]}{E_n^2} \right]. \tag{33}$$

To obtain Eq. (33), we have neglected all terms $\mathcal{O}(E_{01}/E_{\min})$, restated the matrix elements in the basis of the localized Majorana wave functions, and exploited the charge conjugation symmetry one more time to reduce the summation to continuum states with positive energy ($n > 0$).

III. NONADIABATIC LIMITATIONS FOR A QUANTUM WIRE

To study the limitations on topological quantum computing caused by nonadiabatic effects, we now apply the general results (20) and (27) for intrafermionic processes to the quantum wire proposal. Since γ_3 and γ_4 are assumed to be irrelevant for the qubit dynamics, we can focus on the single topological domain depicted in Fig. 3(a). Restricting the analysis to the case where only the positions x_1 and x_2 of the domain walls are varied and taking the localization length ξ of the MBS wave functions to be much shorter than their separation $L = x_2 - x_1$, one can write

$$\mathcal{M}_{\gamma_j,n}(t) \simeq i\,\dot{x}_j(t)\, b_{\gamma_j,n}(L(t)), \tag{34}$$

where the geometric matrix elements are defined by $b_{\gamma_j,n} := \langle\phi_{\gamma_j}|\partial_{x_j}\phi_n\rangle$. The time dependence of x_1 and x_2 may generally be due to random gate fluctuations or the consequence of intentional successive tuning of local gate voltages for the purpose of information processing.

Focusing first on the simplest case $\dot{x}_1 = 0$, Eqs. (20) and (27) are solely determined by I_2, where

$$I_j = \sum_{n>0} \left| \int_{t_0}^{t} dt' \dot{x}_j(t')\, b_{\gamma_j,n}(L(t')) e^{-i\int_{t_0}^{t'} dt_1 E_n(t_1)} \right|^2. \tag{35}$$

The decoherence function reads as $\Gamma = -I_2/2$ and I_2 represents, at the same time, the probability of changing the single-fermion parity. To evaluate I_2, we first need to calculate the geometric matrix elements for the specific setup under discussion. A nanowire with spin-orbit coupling in proximity to an s-wave superconductor can be described by the BdG Hamiltonian[6,7]

$$h_{\text{NW}} = \left(\frac{p^2}{2m} - \mu(x) + up\,\sigma_y\right)\tau_z + B\sigma_z - \Delta\tau_x, \tag{36}$$

where the Pauli matrices σ_j and τ_j act on spin and particle-hole space, respectively. Here, m denotes the effective mass, u the spin-orbit coupling strength, Δ the induced pairing potential, and B the Zeeman energy. This system belongs to class BDI,[17] since, apart from possessing a charge conjugation symmetry with $\Xi^2 = \mathbb{1}$, the Hamiltonian commutes with the generalized time-reversal operator $\Theta = \mathcal{K}$ satisfying $\Theta^2 = \mathbb{1}$. Notice that

the presence of the superconductor is only accounted for by the effective pairing strength Δ. Consequently, additional energy splitting effects caused by the quasiparticle degrees of freedom in the s-wave superconductor[23] are neglected in the following analysis.

A. Large magnetic fields and infinite potential well

To obtain analytical results, we focus on the limit where the magnetic field is the largest energy scale of the topological segment, i.e., $B \gg \epsilon_{so}, \Delta$ with $\epsilon_{so} = mu^2/2$ representing the spin-orbit energy. Under these assumptions, one can project Eq. (36) onto its lower band [green line in Fig. 3(b)] yielding[8]

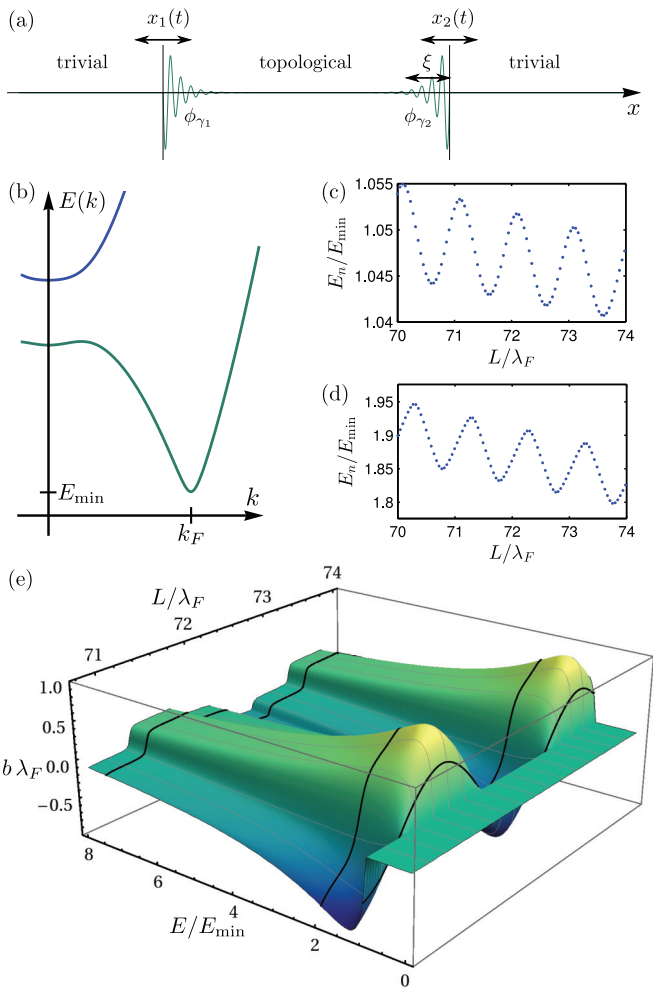

FIG. 3. (Color online) Due to the assumption of intrafermionic manipulation, it is sufficient to analyze an isolated topological segment (a) of the wire surrounded by a trivial phase. In (b), the excitation spectrum of the BdG Hamiltonian (36) for large magnetic fields ($B \gg \epsilon_{so}, \Delta$) is shown. The lower band (green) is effectively described by Kitaev's spinless model (37). In (c) and (d), we show the L dependence of the instantaneous energies of two different states determined numerically from h_{NW} for $B/\Delta = 5$, $B/\epsilon_{so} = 20$, and taking $\mu = 0$ in the topological segment. In (e), the analytical expression (A1) for the geometric matrix elements is plotted as a function of the length L of the topological domain and the energy E of the excited state using the same parameters as in (c) and (d).

the (continuum limit of the) Kitaev model[3]

$$h_{\text{Kit}} = \left(\frac{p^2}{2m} - \mu_e(x)\right)\tau_z - v_e p\,\tau_y \tag{37}$$

as an effective low-energy theory, where $\mu_e = \mu + B$ and $v_e = u\Delta/B$.

Let us first consider an infinite potential well, i.e., we need to find the eigenstates ϕ of Eq. (37) with $\mu_e(x) = \mu_1 > 0$ subject to the constraint $\phi(x_1) = \phi(x_2) = 0$. One can derive an analytical expression (see Appendix A) for the geometric matrix elements taking the energies of the continuum states ϕ_n, $n > 0$, as a continuous quantity E and considering the limit $L \gg \xi, \lambda_F$, where $\lambda_F = 2\pi/k_F$ denotes the Fermi wavelength. Here, we simply show a plot of the result as a function of the system length L and energy E [see Fig. 3(e)] and discuss its relevant properties. Most importantly, the matrix elements exhibit an oscillatory behavior as a function of L with periodicity of $2\lambda_F$ besides the expected slowly varying envelope function $\propto 1/\sqrt{L}$. The latter can hardly be seen in Fig. 3(e). Directly above the gap [rightmost black curve in Fig. 3(e)], the geometric matrix elements are nearly sinusoidal functions of L. However, already at $E/E_{\min} = 2$ (middle black curve) the sinusoidal shape is significantly deformed. For even higher energies (leftmost black line) smaller than but comparable with μ_1 the matrix elements exhibit a rather step-function-like L dependence. By studying the four-component model in Eq. (36) numerically, we have verified that this is not an artifact of the low-energy Hamiltonian (37). The amplitude of the L oscillations of the matrix elements approaches zero in a nonanalytic way ($\propto\sqrt{E - E_{\min}}$) as $E \to E^+_{\min}$, reaches its maximum at approximately $E/E_{\min} = 1.7$ for the parameters used in Fig. 3(e), and then decays monotonically for larger energies.

In Figs. 3(c) and 3(d), the numerically determined L dependence of the instantaneous energies of a state directly above the gap and at a higher energy is shown. We again encounter an oscillatory contribution on top of the usual $1/L^2$ decay (this time with periodicity λ_F). The ratio of its amplitude to the mean energy value increases with energy and decays as $\propto 1/L$.

The oscillation of the energies, which on its own can give rise to transitions,[31] and the complicated functional form of $b_{\gamma_2}(E, L)$ in Eq. (A1) make a quantitative analytical evaluation of I_2 in Eq. (35) very difficult. Nonetheless, we can extract the qualitative behavior of the system from the results presented above. This is achieved as follows. From Eq. (35), it is immediately clear that nonadiabatic effects will contribute significantly when the geometric matrix elements have nonvanishing spectral weight for frequencies $\omega \gtrsim E_{\min}$. Due to the sinusoidal behavior of $b_{\gamma_2}(L)$ for low energies, we conclude that

$$v_c = \frac{2E_{\min}}{k_F} \simeq 2v_e \simeq 2u\frac{\Delta}{B} \tag{38}$$

is the critical velocity scale separating the regimes of nearly adiabatic manipulation ($\dot{L} \ll v_c$) and $\dot{L} \gtrsim v_c$, where nonadiabatic effects render the qubit unstable. Except for the factor of 2 in Eq. (38), the Landau criterion would yield the same result for the critical velocity. Note, however, that Landau's argumentation can not be applied in the present case since only

one bound state is moving. In Sec. IV A, we investigate the situation where the two MBS move with the same velocity, making the application of Landau's criterion possible and hence yielding a critical velocity without an additional factor of 2 [see Eq. (57)].

Let us now estimate the practical relevance of the critical velocity v_c for topological quantum computation. For retaining the topological protection during a braiding process, the MBS have to be separated by a distance which is at least a few times larger than their spatial decay length $\xi \simeq (mv_e)^{-1}$. Consequently, the Majorana modes are to be transported over a distance $\Delta x \simeq \alpha/(mv_e)$ with $\alpha \simeq 10$–100 depending on the braiding operation to be realized. According to Eq. (38), adiabaticity requires the braiding time T_b to satisfy

$$T_\mathrm{b} \gg \frac{\Delta x}{v_c} \simeq \frac{\alpha}{2mv_e^2} \simeq \frac{\alpha}{4\epsilon_\mathrm{so}}\left(\frac{B}{\Delta}\right)^2. \tag{39}$$

We emphasize the difference to the "standard guess" of $T_\mathrm{b} \gg 1/E_\mathrm{min}$ which is much less restrictive since $\Delta x k_F \gg \Delta x/\xi \gg 1$ in the considered limit of large magnetic fields.

Applying recent experimental data[32] and assuming an order-of-magnitude difference between the critical braiding time and the lower bound for T_b, one finds $T_\mathrm{b} > 10^{-8}$ s for $\alpha \simeq 50$. Note that this is already of the same order as the upper bound $T_\mathrm{b} < 10^{-7} - 10^{-8}$ s due to quasiparticle poisoning for the system under discussion.[33] We conclude that nonadiabatic effects due to the presence of degrees of freedom above the gap are not only irrelevant corrections of purely academic interest, but may provide serious challenges for the realizability of topological quantum computing. Note that the authors of Ref. 33 came to a similar conclusion, however, using $T_\mathrm{b} \gg 1/E_\mathrm{min}$ and assuming a much smaller gap than that reported in Ref. 32.

To discuss the typical scaling behavior of the nonadiabatic corrections in the regime $\dot{L} \ll v_c$, let us investigate the prototypal trajectory

$$L(t) = L(0) + \frac{\Delta x}{\pi}\arctan(t/\tau). \tag{40}$$

Assuming that the physics is mainly described by the contribution of the states directly above the gap, we can use the sinusoidal matrix elements $b_{\gamma_2}(L)$. Furthermore, let us neglect the L dependence of the instantaneous energies which can always be justified by choosing L sufficiently large. Upon defining $\beta := \Delta x/(2\lambda_F)$, which measures the number of oscillations of the geometric matrix elements during the trajectory, and $v_\mu := \sqrt{2\mu_1/m}$, one finds

$$I_2 \sim \frac{1}{4\sqrt{2\pi}}\sqrt{\mu_1\tau}\sqrt{\frac{v_e}{v_\mu}}\left(\frac{\Delta x/\tau}{v_e}\right)^2\left(\frac{(2E_\mathrm{min}\tau)^\beta}{\Gamma(1+\beta)}\right)^2 e^{-2E_\mathrm{min}\tau}, \tag{41}$$

as $E_\mathrm{min}\tau, v_\mu/v_e \to \infty$, i.e., for adiabatically slow manipulation and large magnetic fields. Note that the integral depends on Δx and τ independently, which physically stems from the fact that the system not only has an intrinsic time scale $1/E_\mathrm{min}$, but also a length scale λ_F.

Most importantly, we have found that the nonadiabatic corrections decay exponentially as a function of $E_\mathrm{min}\tau$. However, in the adiabatic regime ($\beta < E_\mathrm{min}\tau$), the β-dependent prefactor in Eq. (41) is exponentially large in absolute terms but subleading with respect to $e^{-2E_\mathrm{min}\tau}$. We emphasize that the exponential scaling behavior is directly related to the realistic choice of an analytic protocol $L(t)$. The nonadiabatic corrections to the fermion parity reported in Ref. 13 vanish only algebraically as the braiding velocity approaches zero since the authors assumed a discontinuous velocity profile.

These results indicate that it may be favorable to keep the length L of the topological domain constant during a braiding process, i.e., $\dot{x}_1 = \dot{x}_2$. In this case, both I_1 and I_2 are required to estimate the decoherence effects in Eqs. (20) and (27a). Note that, although the second line of Eq. (20) is not directly determined by I_1 and I_2, its magnitude is bound by $2\sqrt{I_1 I_2}$. Consequently, $I_j \ll 1$ serves as a sufficient condition for adiabatic manipulation. On top of that, the term in the second line of Eq. (20) represents an interference effect between two remote MBS and hence it is expected to be negligible[34] compared to the first line for well-separated Majorana modes.

Since both the geometric matrix elements and the instantaneous energies are constant, the evaluation of I_j is now readily performed analytically. We obtain for the trajectory (40) in the limit $v_\mu/v_e \to \infty$

$$I_1 = I_2 \sim \frac{1}{2\sqrt{2\pi}}\sqrt{\mu_1\tau}\sqrt{\frac{v_e}{v_\mu}}\left(\frac{\Delta x/\tau}{v_e}\right)^2 e^{-2E_\mathrm{min}\tau}. \tag{42}$$

Note that Eq. (42) is independent of L which is a consequence of the summation over the different states of the continuum. This result implies that parity errors and decoherence effects due to nonadiabatic processes are exponentially suppressed as $e^{-2E_\mathrm{min}\tau}$ and consequently lead to the weaker constraint $\tau \gg \tau_c = 1/E_\mathrm{min}$ for adiabatic quantum computation, as compared to the case of one moving MBS. The stark difference between braiding with constant system length L and moving only one Majorana mode physically stems from the fact that the continuum states extend over the entire topological segment of the wire. Although describing the local coupling of a MBS to an excited mode, the geometric matrix elements can thus depend on L. Naturally, this picture is only valid as long as the wire is sufficiently clean such that the mean-free path is larger than the wire length L, which is assumed throughout this paper.

B. Large spin-orbit coupling

So far, we have analyzed the wire Hamiltonian (36) only in the limit of strong magnetic fields ($B \gg \epsilon_\mathrm{so}, \Delta$). However, also the regime where the spin-orbit coupling at the Fermi level is much larger than the magnetic field and the proximity pairing strength, i.e., $\epsilon_\mathrm{so} \gg B, \Delta$, is appropriate for engineering MBS. For $\mu = 0$ the gap at the Fermi wave vector $k_F \simeq 2mu$ is approximately given by Δ. Sufficiently far away from the topological phase transition (explicitly for $B > 2\Delta$) the minimal gap in the system occurs at k_F.

We have shown by diagonalizing $h_\mathrm{NW}(L)$ numerically that, also in this limit, the geometric matrix elements $b_{\gamma_j,n}$ are sinusoidal functions of L with periodicity $2\lambda_F$ in the vicinity of the gap and become increasingly deformed for higher energies, similarly to Fig. 3(e). The decay length of the Majorana wave function is given by u/Δ in the present regime of the nanowire[35] and thus the critical velocity as well as the

associated restriction on T_b read as

$$v_c = \frac{2E_{\min}}{k_F} \simeq u\frac{\Delta}{2\epsilon_{so}}, \quad T_b \gg \frac{\Delta x}{v_c} \simeq \frac{2\alpha}{\epsilon_{so}}\left(\frac{\epsilon_{so}}{\Delta}\right)^2, \quad (43)$$

respectively. Note that this result has the same structure as Eq. (39) obtained in the limit of large B upon replacing the ratio B/Δ by ϵ_{so}/Δ and hence the lower boundaries for T_b are expected to be of the same order in both regimes of the nanowire.

IV. QUANTUM COMPUTING USING NONADIABATIC EFFECTS

In the previous section, nonadiabatic effects have been treated solely as a drawback for topological quantum computing. However, they may also be regarded as an opportunity for constructing additional gate operations. In the following, we analyze how nonadiabatic processes can be used to realize a phase gate $\exp(i\varphi\sigma_z/2)$, and thus, as a special case, a $\pi/8$ gate ($\varphi = \pi/4$), the missing single qubit gate for universal quantum computation.[27]

By combining Eqs. (23) and (31), we find that the phase φ accumulated during a manipulation of the system can be written as

$$\varphi = \int_{-\infty}^{\infty} dt' \, [E_{01}(t') + \delta E(t')] \quad (44)$$

in the regime of nearly adiabatic manipulation defined by Eq. (29). This is the limit of interest since a proper gate operation conserves the fermion parity and the coherence of the qubit. Note that, by construction, Eq. (44) can be retrieved directly from the more general expression (27b) by a formal expansion in the small parameters in Eq. (29).

The most obvious way for controllably generating a phase φ would be to use the tunnel splitting E_{01}, i.e., to bring the MBS close together for a certain amount of time. This approach has already been analyzed intensively in the past.[36,37] Here, we ask whether it is possible to use the nonadiabatic energy splitting δE to accumulate a well-defined phase without having direct overlap of the Majorana wave functions.

For this purpose, let us rewrite the leading term of the energy correction (32) as

$$\delta E = -\langle\dot\phi_{01}(t)|G|\dot\phi_{01}(t)\rangle \times \left[1 + \mathcal{O}\left(\frac{E_{01}}{E_{\min}}\right)\right] \quad (45)$$

$$= \mathrm{Im}\left[\langle\dot\phi_{\gamma_2}(t)|G|\dot\phi_{\gamma_1}(t)\rangle\right] \times \left[1 + \mathcal{O}\left(\frac{E_{01}}{E_{\min}}\right)\right], \quad (46)$$

where we have introduced the Green's function

$$G = \sum_n \frac{|\phi_n(t)\rangle\langle\phi_n(t)|}{E_n} \quad (47)$$

of the BdG Hamiltonian $h(t)$. To obtain the summation over all states in Eq. (47), we have used the parallel transport phase convention (5) and $\langle\phi_{01}|\partial_t\phi_{\overline{01}}\rangle = 0$. Since the nonadiabatic accumulation of a phase is a correlation effect between spatially separated MBS (see Sec. II B), the appearance of a Green's function is quite natural. By calculating the Green's function G for the case of the infinite potential well described by the Kitaev model (37), we have shown that the energy correction δE in Eq. (46) is exponentially small ($e^{-L/\xi}$) in the separation L of the MBS. This was to be expected since G describes the (zero-frequency) propagation in a gapped system and thus decays exponentially in space. Taking into account the zero-energy boundary modes does not change this conclusion. Note that $\mathcal{M}_{\gamma_1,n}\mathcal{M}^*_{\gamma_2,n} \in i\,\mathbb{R}$ for the Kitaev model and hence the second line of Eq. (33) vanishes entirely. Consequently, also the next-order contribution to the nonadiabatic energy splitting [second term in Eq. (32)] is at least of linear order in $E_{01}/E_{\min} \propto e^{-L/\xi}$.

We have seen that the topological protection of the qubit, due to the separation of the MBS, also holds for the virtual processes in the regime of nearly adiabatic manipulation. Therefore, in order to implement a phase gate according to Eq. (44), one has to either bring the Majorana modes close together such that L is of order ξ or use sufficiently high velocities, where the perturbative approach in $\mathcal{M}$ breaks down. In this paper, we study the latter option.

A. Parallel translation of two MBS

From Sec. III we know that the coherence and the fermion parity of the topological qubit are most stable against large braiding velocities, if the system length L is held constant. For this reason, let us now focus on the case $\dot x_1(t) = \dot x_2(t) =: v(t)$, which, in addition, provides an alternative way of treating nonadiabatic effects.

1. Next adiabatic iteration

To see this, let us introduce the spatial displacement operator

$$\mathcal{W}(t) = \mathbb{1}\, e^{-ip\int_{t_0}^{t} dt' v(t')}, \quad (48)$$

where $\mathbb{1}$ denotes the identity matrix both in spin and particle-hole space. This enables us to write

$$h(t) = \mathcal{W}(t)h(t_0)\mathcal{W}^\dagger(t) \quad (49)$$

and, consequently, the instantaneous eigenstates satisfy $|\phi_n(t)\rangle = \mathcal{W}(t)|\phi_n(t_0)\rangle$. Therefore, the corresponding "moving frame" BdG Hamiltonian is simply given by

$$h'(v(t)) = h(t_0) - i\,\mathcal{W}^\dagger(t)\dot{\mathcal{W}}(t) \quad (50)$$

$$= h(t_0) - \mathbb{1}\, v(t)\, p, \quad (51)$$

which determines the entire dynamics of the system by means of Eq. (14). Note that we have found an explicit form of h' without having to calculate entries of the coupling matrix $\mathcal{M}$ explicitly.

Instead of applying perturbation theory in the second term in Eq. (51), i.e., in the velocity v, let us follow an approach which essentially goes back to Ref. 38 and diagonalize $h'(v)$ for every v:

$$h'(v)|\phi'_n(v)\rangle = E'_n(v)|\phi'_n(v)\rangle. \quad (52)$$

Since v is only a one-dimensional parameter, we can use again the parallel transport condition $\langle\phi'_n|\partial_v\phi'_n\rangle = 0$ to remove the phase ambiguity between the (single-valued) superadiabatic eigenfunctions $|\phi'_n(v)\rangle$ at different values of v. Similar to Eq. (12), the Hamiltonian governing the time evolution in the

superadiabatic basis is given by

$$h''_{n,m}(t) = E'_n(v(t))\delta_{n,m} - \mathcal{M}'_{n,m}(t), \tag{53}$$

where the new coupling matrix elements read as

$$\mathcal{M}'_{n,m}(t) = i\,\dot{v}(t)\langle\phi'_n(v(t))|\partial_v\phi'_m(v(t))\rangle. \tag{54}$$

For any realistic translation process, we have $v(t) \to 0$ as $|t| \to \infty$. Under this assumption, it is easily seen that the matrix exponential defined in Eq. (14) obeys for $t_0 \to -\infty$ and $t \to \infty$:

$$u_{n,m} = \left[\mathcal{T}\exp\left(-i\int_{-\infty}^{\infty} dt'\,h''(t')\right)\right]_{n,m}. \tag{55}$$

In straightforward analogy, the perturbative analysis of Secs. II B and II C can now be repeated in the superadiabatic basis. Since $\mathcal{M}' \propto \dot{v}$, this yields results which are perturbative in the acceleration but contain v to arbitrary order making the regime of large velocities accessible.

2. *Quantum wire at strong magnetic fields*

Again, let us focus on the regime of large magnetic fields $B \gg \epsilon_{\rm so}, \Delta$, where the system can be effectively described by Kitaev's model (37) and hence the "moving frame" Hamiltonian reads as

$$h'_{\rm Kit}(v) = \left(\frac{p^2}{2m} - \mu_e(x)\right)\tau_z - v_e\,p\,\tau_y - \mathbb{1}\,v\,p. \tag{56}$$

The resulting excitation spectrum $E'(k)$ is illustrated in Fig. 4(a). We observe that the presence of the additional term vp in the BdG Hamiltonian tilts the dispersion and drives the system into a gapless phase for

$$v > v^* \simeq v_e \simeq \frac{u\Delta}{B}. \tag{57}$$

The system is very sensitive to small accelerations when the velocity v^* is reached since the superadiabatic gap $E'_{\rm min}(v)$ closes for $v \to v^*$. Therefore, we recover the concept of a critical velocity scale also for the entirely translated system. In the present case, however, the qubit will still be protected from decoherence for sufficiently small $\dot{v}$, even if v becomes comparable with v^*.

To understand how the superadiabatic MBS behave when the velocity v is increased, let us investigate the four possible wave vectors $\{\pm q'_+, \pm q'_-\}$ of the Majorana wave functions. For constant $\mu_e(x) = \mu_1 > 0$, one finds from Eq. (56)

$$q'_\sigma(v) \simeq m v_e\sqrt{1-(v/v_e)^2} + \sigma\, i\sqrt{2m\,\mu_1} \tag{58}$$

for vanishing tunnel splitting $E'_{01}(v) = 0$, i.e., assuming an infinitely long topological domain. Since $\mathrm{Re}[q'_\sigma(v)]$ decreases with v, the MBS wave functions broaden when the system is accelerated. The tunnel splitting becomes significant above a certain velocity $v < v^*$ for any finite length L of the topological domain because $\mathrm{Re}[q'_\sigma(v)]$ approaches 0 as $v \to v^*$. Thus, we expect that the associated ground-state eigenfunctions $|\phi'_{01}\rangle$ and $|\phi'_{\overline{01}}\rangle$ finally merge into the continuum for $v \gtrsim v^*$.

For a more quantitative picture, the moving frame Hamiltonian $h'(v)$ in Eq. (51) is diagonalized numerically using the full four-component BdG Hamiltonian (36) of the nanowire. We again take a piecewise constant chemical potential to describe the domain walls between the topological ($\mu = 0$) and trivial ($\mu = \mu_2 < -\sqrt{B^2 - \Delta^2}$) phases illustrated in Fig. 3(a).

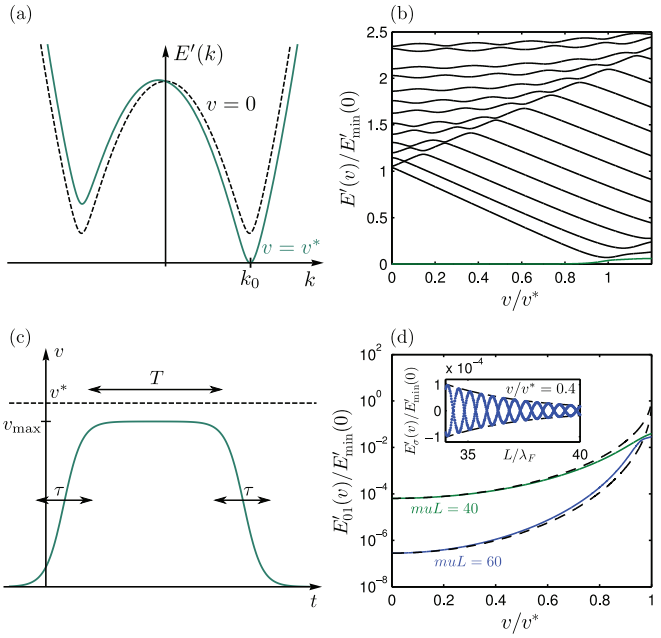

FIG. 4. (Color online) (a) Excitation spectrum of the "moving frame" Kitaev model (56) for $v = 0$ (black dashed line) and right at the critical velocity v^* (green line) at which the system becomes gapless. In (b), numerical results for the energy splitting (green) and for the energies of the first states above the gap (black) as a function of the velocity v are shown. Here, we used the moving frame Hamiltonian of the wire Hamiltonian (36) with $B/\Delta = 4$, $B/\epsilon_{\rm so} = 25$, $muL = 40$, and $\mu_2 = -10B$. Part (c) illustrates the suggested velocity profile for realizing a nonadiabatic phase gate. In (d), we show numerical results for the energies of the ground-state fermions as a function of the velocity v for two different system lengths and as a function of L for a fixed value of v (inset). Here, the same parameters as in (b) have been used. The black dashed lines correspond to the expected scaling behavior in Eq. (61).

Figure 4(b) shows the resulting energies of the first excited states above the gap and the tunnel splitting E'_{01} as a function of the velocity v. As expected, the energies of the excited states are reduced with increasing v (with a slope approximately given by k_F in the linear regime) and the fermionic ground-state solutions of $h'(0)$ smoothly connect to the ordinary states of the quasicontinuum at $v \simeq v^*$.

For a concrete implementation of a phase gate, let us investigate the protocol illustrated in Fig. 4(c), which is characterized by the two time scales τ and T representing the acceleration time and the time during which the maximum velocity $v_{\rm max} < v^*$ is held constant.

In analogy to Eq. (44), the phase φ accumulated during the processes can be written as $\varphi = \varphi_1 + \varphi_2$, where

$$\varphi_1 = \int_{-\infty}^{\infty} dt_1\, E'_{01}(v(t_1)) \tag{59}$$

is the dynamical phase in the superadiabatic basis and φ_2 the acceleration correction. Applying the approximative projection procedure presented in Sec. II C to the superadiabatic

Hamiltonian (53), one finds

$$\varphi_2 \simeq -\sum_{n\neq 0}\int_{-\infty}^{\infty} dt\ \dot{v}^2\ \frac{|\langle\phi'_{01}(v)|\partial_v\phi'_n(v)\rangle|^2}{E'_n(v)-E'_{01}(v)} \tag{60}$$

valid for small $\dot{v}$.

To begin with the dynamical phase φ_1, numerical results for the tunnel splitting $E'_{01}(v)$ as a function of the velocity are shown in Fig. 4(d) for two different values of the system length L. As expected from the analysis of the virtual energy correction (45) in the adiabatic basis, large velocities comparable with v^* are to be applied to generate a significant increase in $E'_{01}(v)$. Since the gate operation time has to be much shorter than the time scale $1/E'_{01}(0)$ on which the phase of ρ^Q_{01} is modified due to the tunnel splitting at $v=0$, we require $E'_{01}(v_{\max})/E'_{01}(0) \gg 1$. Focusing on $muL = 60$, the numerical data in Fig. 4(d) imply that one has to choose $v_{\max}/v^* = 0.8$ such that $E'_{01}(v_{\max})/E'_{01}(0)$ is of order 10^2–10^3.

At least for sufficiently small $E'_{01}(v)$, the envelope function of E'_{01} is expected to scale as $\exp\{-\mathrm{Re}[q'_\sigma(v)]L\}$, where $q'_\sigma(v)$ is given by Eq. (58). Fitting the prefactor to the numerical data yields good agreement for the scaling behavior of E'_{01} as a function of both v and L as can be seen from the black dashed lines in Fig. 4(d). For that reason,

$$\frac{E'_{01}(v_{\max})}{E'_{01}(0)} \propto e^{(\mathrm{Re}[q'_\sigma(0)]-\mathrm{Re}[q'_\sigma(v_{\max})])L} \tag{61}$$

is to be expected and hence the enhancement of the energy splitting can be easily enlarged by increasing the system length L.

To avoid decoherence and parity errors, τ has to be chosen much larger than the time scale $\tau_c = 1/E'_{\min}(v_{\max})$. Assuming that $v_{\max}/v^* = 0.8$, we find $\tau_c \simeq 5/E'_{\min}(0)$ from Fig. 4(b). In order to investigate the relevance of the contribution of φ_2, we have calculated the scalar products and the summation in Eq. (60) numerically. Again, referring to $v_{\max}/v^* = 0.8$ and $muL = 60$, one finds $\varphi_2/(2\pi) < 10^{-2}$ for $\tau \gtrsim 10^2\tau_c$. Consequently, with these parameters not only the coherence and the parity of the qubit are expected to be unaffected, but also $\varphi \simeq E'_{01}(v_{\max})T$ with corrections due to the acceleration which are smaller by a factor of order 10^{-2}. In principle, however, one could also take the acceleration corrections into account by properly calibrating the phase gate.

The inset in Fig. 4(d) shows the energies $E'_\sigma(v)$, $\sigma = 01, \overline{01}$, for $v = 0.4\,v^*$ as a function of L. We observe that the superadiabatic tunnel splitting is sinusoidal in L with periodicity given by the Fermi wavelength λ_F as is well known for the adiabatic tunnel splitting.[22,36] This means that L has to be stabilized with an accuracy on the length scale λ_F for a controllable manipulation of the phase of ρ^Q_{01}. Note that this problem can be overcome in the scheme based on the direct overlap of the MBS wave functions by using their monotonically decaying behavior in the nontopological domains of the wire.[36] Unfortunately, this solution of the problem is not readily transferred to our proposal. Nevertheless, we believe that the notion of a nonadiabatic phase gate may not only be of theoretical interest because it represents an alternative that might be helpful for making potential quantum computation schemes to work more efficiently. Furthermore, the approach presented here may be seen as a starting point for the search of more sophisticated procedures of constructing gate operations based on nonadiabatic effects. In the following section, we present a first example of a proposal that is easier accessible experimentally.

B. Manipulations by supercurrent

The analysis presented above has shown that a phase gate which does not require bringing the MBS close to each other is in principle possible by taking advantage of nonadiabatic effects. Although the error threshold is very large (14%) due to a correction scheme known as "magic-state distillation,"[26,39] the experimental implementation may be complicated since high velocities of order v^* are required, while L has to be fixed with high accuracy ($\delta L \ll \lambda_F$). Therefore, let us investigate a related setup, first studied in Ref. 40, where instead of moving the MBS relative to the s-wave superconductor, a supercurrent $J(t)$ is driven through the proximity-inducing superconductor along the nanowire.

The presence of the current induces a gradient $\partial_x\varphi(x,t)$ in the phase of the superconducting order parameter Δ in Eq. (36) according to $J(t) \propto \partial_x\varphi(x,t)$. Focusing on the case where $J(t)$ is spatially uniform and applying a suitable gauge transformation,[40] the Hamiltonian can be written as

$$\begin{aligned}\widetilde{h}_{\mathrm{NW}}(\partial_x\varphi) &= \left\{\frac{1}{2m}\left[p^2+\left(\frac{\partial_x\varphi}{2}\right)^2\right]-\mu+u\left(p-\tau_z\frac{\partial_x\varphi}{2}\right)\sigma_y\right\}\tau_z \\ &\quad + B\sigma_z - \Delta\tau_x - \frac{\partial_x\varphi}{2m}p.\end{aligned} \tag{62}$$

For a derivation of the resulting phase diagram for time-independent currents, we refer the reader to Ref. 40. Here, we will only discuss the applicability of this system for implementing a phase gate.

1. *Limit of large magnetic fields*

As before, we first analyze the regime of strong magnetic fields. It is instructive to compare Eq. (62) with the moving frame Hamiltonian

$$h'_{\mathrm{NW}}(v) = \left(\frac{p^2}{2m}-\mu+up\,\sigma_y\right)\tau_z + B\sigma_z - \Delta\tau_x - v\,p \tag{63}$$

for the spatially displaced topological domain. We observe that the last terms in Eqs. (62) and (63) are identical upon identifying $v = \partial_x\varphi/(2m)$. For low energies $E \ll B$ and $v < v^*$, the momenta of the excited states of $h'_{\mathrm{NW}}(v)$ are of order of the Fermi wave vector $k_F \simeq \sqrt{2mB}$ [see Fig. 4(a)]. Since $|q'_\sigma(v)| \gtrsim k_F$, the Hamiltonians in Eqs. (62) and (63) are identical for low energies as long as $\partial_x\varphi \ll k_F$. According to the identification $v = \partial_x\varphi/(2m)$ and using Eq. (57), the critical phase gradient is given by

$$(\partial_x\varphi)^* = 2mv^* \simeq \frac{2mu\Delta}{B}, \tag{64}$$

which indeed satisfies $(\partial_x\varphi)^* \ll k_F$. For this reason, $\widetilde{h}_{\mathrm{NW}}(\partial_x\varphi)$ and $h'_{\mathrm{NW}}(v)$ with $v = \partial_x\varphi/(2m)$ exhibit the identical low-energy behavior for the entire topological regime. Therefore, we know that the system undergoes a transition at $(\partial_x\varphi)^*$ from a topological phase into a gapless phase in accordance with the results of Ref. 40. Moreover, the numerical data shown in

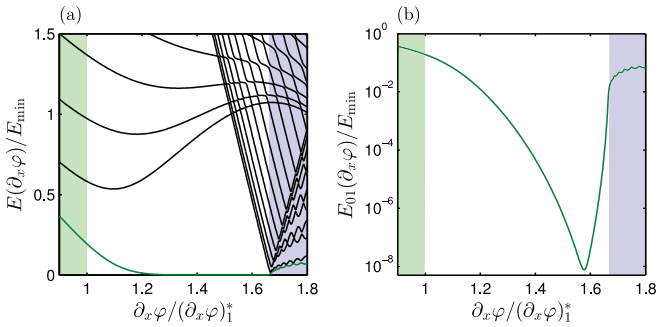

FIG. 5. (Color online) (a) Excitation energies of Eq. (62) for different values of the phase gradient $\partial_x\varphi$ obtained numerically using $B/\Delta = 0.9$, $\epsilon_{so}/\Delta = 0.5$, $muL = 80$, and taking $\mu = 0$ in the topological segment of the wire. The trivial and gapless phases are highlighted in green and blue, respectively. $E_{\min}$ is defined as the maximum gap in the topological phase. In (b), the tunnel splitting is shown again on a logarithmic scale.

Fig. 4 and the resulting estimates in Sec. IV A also hold for this setup upon replacing v/v^* by $\partial_x\varphi/(\partial_x\varphi)^*$. As a consequence, supercurrents can be used similar to the translation of the topological domain for realizing a phase gate without bringing MBS closer together.

On top of that, we believe that driving supercurrents along the nanowire may be easier to implement experimentally since no local gate tuning is required. Furthermore, the stabilization of the length of the topological domain is expected to be less problematic, if the position of both MBS is fixed.

2. *Current-induced topological phase*

By applying a supercurrent along the nanowire, it is even possible to stabilize a topological phase when $B < \Delta$, for which the system would reside in the trivial phase, if no current was present. Clearly, this can not be achieved by simply translating the system since the additional term vp in Eq. (51) leaves the topological gap at $k = 0$ unaffected.

In Fig. 5(a), numerical results for the excitation energies of the BdG Hamiltonian (62) with $B/\Delta = 0.9$ and $\epsilon_{so}/\Delta = 0.5$ are shown as a function of the gradient $\partial_x\varphi$. We know from Ref. 40 that for these parameters one can realize a trivial $[\partial_x\varphi < (\partial_x\varphi)_1^*]$, a topological $[(\partial_x\varphi)_1^* < \partial_x\varphi < (\partial_x\varphi)_2^*]$, and a gapless phase $[\partial_x\varphi > (\partial_x\varphi)_2^*]$ by tuning the strength of the phase gradient. As expected, the quasi-zero-energy modes of the topological domain merge into the continuum for $\partial_x\varphi \lesssim (\partial_x\varphi)_1^*$ and $\partial_x\varphi \gtrsim (\partial_x\varphi)_2^*$. On the one hand, the transition to the gapless phase at $(\partial_x\varphi)_2^*$ is similar to the behavior found in Fig. 4(b) for the system displaced with velocity $v \lesssim v^*$. The gap is strongly reduced for $\partial_x\varphi \to (\partial_x\varphi)_2^*$ compared to its maximum value $E_{\min}$ at $\partial_x\varphi \simeq 1.5(\partial_x\varphi)_1^*$. On the other hand, when $\partial_x\varphi$ approaches $(\partial_x\varphi)_1^*$ from above, the gap is reduced only by a factor of 2, making the qubit much less sensitive to parity errors and decoherence effects. Clearly, this is a finite-size effect and reflects the fact that the density of states of the nontopological phase is much smaller than that of the gapless phase. However, as far as the topological protection of the qubit is concerned, the system length only has to be sufficiently large compared to the localization length of the MBS such that the tunnel splitting E_{01} is negligible. From Fig. 5(b), we can see that E_{01} assumes a minimum value of order $10^{-8}E_{\min}$ slightly below $\partial_x\varphi = 1.6(\partial_x\varphi)_1^*$. By tuning the supercurrent to this minimum, the topological memory can be stored on a time scale which is 7–8 orders of magnitude larger than the scale $1/E((\partial_x\varphi)_1^*) \simeq 4/E_{\min}$ associated with adiabaticity during a phase gate operation based on approaching the boundary $(\partial_x\varphi)_1^*$ to the nontopological phase.

V. CONCLUSIONS

In this work, we have studied the nonadiabatic dynamics of a topological qubit due to the presence of a quasicontinuum of degrees of freedom above the gap of the system. To characterize the qubit, the off-diagonal component ρ_{01}^Q of its reduced density matrix as well as the parity $\hat{\mathcal{P}}_{01}$ of the fermion associated with γ_1 and γ_2 have been considered. We discussed both aspects of nonadiabatic effects, the limitations they impose on topological quantum computation, and the opportunities they provide for creating additional gate operations.

First, a general topological superconductor of class BDI, D, or DIII coupled to a time-dependent classical field has been investigated and perturbative expressions for $\langle\hat{\mathcal{P}}_{01}\rangle$ and ρ_{01}^Q have been derived. Our results show that correlation effects between remote Majorana modes, mediated by the extended states of the continuum, can lead to the accumulation of a phase by the qubit, even if the overlap of their wave functions is small. The derivation of an effective ground-state Hamiltonian for the regime of nearly adiabatic manipulation makes it clear that this phase can be seen as the result of the nonadiabatic renormalization of the tunnel splitting.

In the remainder of the paper, these generic results have been applied to the spin-orbit-coupled nanowire in proximity to an s-wave superconductor assuming that the MBS are transported by varying the chemical potential profile. Focusing on the limit of large magnetic fields, we used Kitaev's model to calculate the relevant coupling matrix elements which turned out to be oscillatory as a function of the length L of the topological domain (with periodicity $2\lambda_F$). This implies a critical velocity scale $v_c \simeq 2E_{\min}/k_F$ for moving one edge of the topological segment of the wire. Our analysis reveals that the resulting lower bound on the braiding time is expected to be of the same order as the upper bound imposed by single-electron tunneling.[33] By taking a prototypal analytic trajectory $L(t)$, we have shown that the nonadiabatic corrections are exponentially suppressed $[\propto \exp(-2E_{\min}\tau)]$ for small velocities $\dot{L} \ll v_c$. In the regime of strong spin-orbit coupling, we found a similar oscillatory behavior of the coupling matrix elements, and the resulting lower bound on the braiding time turned out to be of the same order as in the case of strong magnetic fields.

We then investigated, in detail, the possibility of constructing a nonadiabatic phase gate. Our findings show that a perturbative treatment of the braiding velocities $\dot{x}_j$ of the MBS only leads to nonadiabatic corrections to the tunnel splitting that are exponentially small $[\exp(-L/\xi)]$ in the distance L between the Majorana modes. In order to investigate larger braiding velocities, we assumed that the entire topological domain is translated, making a perturbative calculation with respect to the acceleration possible. We found a critical

velocity v^*, of the same order as v_c above, where the effective "moving frame" Hamiltonian becomes gapless. A trajectory is presented where the relative error of the accumulated phase due to the acceleration parts of the protocol and decoherence effects as well as parity errors are expected to be negligible. However, engineering a nonadiabatic phase gate by translation of the entire topological domain may be difficult in practice since the distance between the MBS has to be well stabilized on the length scale λ_F. This is why we analyzed a different setup,[40] where the position of the MBS is fixed and, instead, a supercurrent is applied along the nanowire. In the regime of strong magnetic fields, the two systems are essentially identical and hence supercurrents can be used similar to the translation of the topological domain for implementing a phase gate. On top of that, supercurrents reveal additional ways for accumulating a phase. For example, in the parameter regime where a topological phase can be stabilized by a current even if $B < \Delta$, we found that finite-size effects can be exploited for efficiently protecting the qubit from decoherence. This shows already that there are various possibilities to improve the most straightforward approach of just translating MBS in order to construct nonadiabatic gate operations. In fact, we believe that this paper might pave the way for the development of more elaborate schemes for the implementation of nonadiabatic phase gates or even of nontrivial two-qubit gates.

Note added. Recently, we became aware of Ref. 41, which shows considerable overlap with our work.

ACKNOWLEDGMENTS

We gratefully thank I. Martin, Y. Makhlin, P. Kotetes, and B. Jeevanesan for various inspiring and useful discussions. A.S. is grateful to the Weizmann Institute of Science (Weston Visiting Professorship) and the BMBF Project No. RUS 10/053 "Topologische Materialien für Nanoelektronik."

APPENDIX: GEOMETRIC MATRIX ELEMENTS

In this appendix, we present the analytical result for the geometric coupling matrix elements $b_{\gamma_2,n} = \langle \phi_{\gamma_2} | \partial_{x_2} \phi_n \rangle$ using the Kitaev model (37) and an infinite potential well.

We introduce the pseudo-parity-operator $\Pi = \tau_z \mathcal{P}$, where $\mathcal{P}$ denotes the spatial inversion with respect to the center of the topological domain, and take advantage of $\Pi^2 = \mathbb{1}$ as well as the fact that Π commutes with the Hamiltonian. Within each of the two eigenspaces of Π associated with eigenvalues $\lambda = \pm 1$, there is a sequence of continuum states with nondegenerate energies E_s^λ, $s \in \mathbb{N}^+$. Let us choose the sequence E_s^λ to be monotonically increasing and define the auxiliary quantum number $\sigma = (-1)^s \lambda$, which turns out to be central in the calculation of $b_{\gamma_2,n}$. Since it is not possible to find an analytical expression for the discrete energies E_s^λ, we treat the energy of the continuum states as a continuous variable E and calculate a smooth interpolating function $b_{\gamma_2}(E)$. In the limit $L \gg \xi, \lambda_F$, we obtain

$$b_{\gamma_2}(E,L) \simeq \frac{\sqrt{2 v_e \mu_1}}{\sqrt{L[1+R^2(E,L)]\,E}} \Bigg[k_-(E)\, \sin\left([k_F - \delta k(E,L)] \frac{L}{2} + \varphi_-(E) \right) + R(E,L)\, k_+(E)\, \sin\left([k_F + \delta k(E,L)] \frac{L}{2} + \varphi_+(E) \right) \Bigg], \tag{A1}$$

where

$$\varphi_\pm(E) := \frac{\theta[k_\pm(E)]}{2} + \arctan\left(\frac{4m^2 v_e^2 + \Omega^2 - k_\pm^2(E)}{4 m v_e k_\pm(E)} \right) \tag{A2}$$

and

$$\delta k(E,L) := \frac{\pi}{L}\, \delta_{\sigma,-1} + \frac{2\,\mathrm{sgn}(\sigma)}{L} \arctan\left(\frac{1}{2(1-g)\tan\left(k_F \frac{L}{2}\right)} \left\{ (1+g)\left[1 + \tan^2\left(k_F \frac{L}{2} \right) \right] - \sqrt{(1+g)^2 \left[1 + \tan^2\left(k_F \frac{L}{2} \right) \right]^2 - 4(1-g)^2 \tan^2\left(k_F \frac{L}{2} \right)} \right\} \right). \tag{A3}$$

In Eqs. (A1)–(A3), the following conventions are being used: The angle $\theta(k) \in [0,\pi)$ is defined via

$$\cos[\theta(k)] = \frac{\mu_1 - \frac{k^2}{2m}}{\epsilon(k)}, \tag{A4}$$

where

$$\epsilon(k) = \sqrt{\left(\frac{k^2}{2m} - \mu_1 \right)^2 + v_e^2 k^2} \tag{A5}$$

is the spectrum of Eq. (37). The Fermi wave vector is given by

$$k_F = \sqrt{2m\left(\mu_1 - m v_e^2\right)} \tag{A6}$$

and coincides with the real part Ω of the wave vectors of the MBS in the physically relevant limit of large magnetic fields ($\mu_1 \gg m v_e^2$). Furthermore,

$$k_\pm(E) = \sqrt{k_F^2 \pm 2m\sqrt{E^2 - E_{\min}^2}} \tag{A7}$$

are the absolute values of the four possible momenta $\{\pm k_+, \pm k_-\}$ of a continuum state with energy $E < \mu_1$. In addition, we defined

$$R = -\frac{\cos\left(\frac{\theta(k_F-\delta k)}{2}\right)}{\cos\left(\frac{\theta(k_F+\delta k)}{2}\right)} \frac{\sin\left[(k_F-\delta k)\frac{L}{2}\right]}{\sin\left[(k_F+\delta k)\frac{L}{2}\right]} \tag{A8}$$

and

$$g(E) = \frac{\tan\{\theta[k_-(E)]/2\}}{\tan\{\theta[k_+(E)]/2\}}. \tag{A9}$$

In Fig. 3(e), this result is shown for $\sigma = +1$. In the second case, $\sigma = -1$, the geometric matrix elements are identical except for a shift by $\lambda_F/2$ in their functional dependence on L.

Exploiting again the pseudoinversion symmetry of the problem, one can easily show that the coupling matrix elements involving the left MBS γ_1 are simply given by $b_{\gamma_1,n} = \pm i\lambda b_{\gamma_2,n}$, where the constant sign $\pm$ depends on how the relative sign between the wave functions ϕ_{γ_1} and ϕ_{γ_2} is chosen.

[1] J. Alicea, Rep. Prog. Phys. **75**, 076501 (2012).
[2] N. Read and D. Green, Phys. Rev. B **61**, 10267 (2000).
[3] A. Y. Kitaev, Phys. Usp. **44**, 131 (2001).
[4] D. A. Ivanov, Phys. Rev. Lett. **86**, 268 (2001).
[5] L. Fu and C. L. Kane, Phys. Rev. B **79**, 161408 (2009).
[6] Y. Oreg, G. Refael, and F. von Oppen, Phys. Rev. Lett. **105**, 177002 (2010).
[7] R. M. Lutchyn, J. D. Sau, and S. Das Sarma, Phys. Rev. Lett. **105**, 077001 (2010).
[8] J. Alicea, Y. Oreg, G. Refael, F. von Oppen, and M. P. A. Fisher, Nat. Phys. **7**, 412 (2011).
[9] K. Flensberg, Phys. Rev. Lett. **106**, 090503 (2011).
[10] B. van Heck, A. R. Akhmerov, F. Hassler, M. Burrello, and C. W. J. Beenakker, New J. Phys. **14**, 035019 (2012).
[11] J. C. Budich, S. Walter, and B. Trauzettel, Phys. Rev. B **85**, 121405 (2012).
[12] G. Goldstein and C. Chamon, Phys. Rev. B **84**, 205109 (2011).
[13] M. Cheng, V. Galitski, and S. Das Sarma, Phys. Rev. B **84**, 104529 (2011).
[14] M. Cheng, R. M. Lutchyn, and S. Das Sarma, Phys. Rev. B **85**, 165124 (2012).
[15] E. Perfetto, Phys. Rev. Lett. **110**, 087001 (2013).
[16] M. J. Schmidt, D. Rainis, and D. Loss, Phys. Rev. B **86**, 085414 (2012).
[17] S. Ryu, A. P. Schnyder, A. Furusaki, and A. W. W. Ludwig, New J. Phys. **12**, 065010 (2010).
[18] A. Saket, S. R. Hassan, and R. Shankar, Phys. Rev. B **82**, 174409 (2010).
[19] W. DeGottardi, D. Sen, and S. Vishveshwara, New J. Phys. **13**, 065028 (2011).
[20] F. L. Pedrocchi, S. Chesi, S. Gangadharaiah, and D. Loss, Phys. Rev. B **86**, 205412 (2012).
[21] Y.-C. He and Y. Chen, arXiv:1210.5139.
[22] M. Cheng, R. M. Lutchyn, V. Galitski, and S. Das Sarma, Phys. Rev. Lett. **103**, 107001 (2009).
[23] A. A. Zyuzin, D. Rainis, J. Klinovaja, and D. Loss, Phys. Rev. Lett. **111**, 056802 (2013).
[24] E_{0j} can have isolated zeros as a function of the spatial separation of the MBS.
[25] M. V. Berry, in *Geometric Phases in Physics*, edited by A. Shapere and F. Wilczek (World Scientific, Singapore, 1989).
[26] S. Bravyi, Phys. Rev. A **73**, 042313 (2006).
[27] C. Nayak, S. H. Simon, A. Stern, M. Freedman, and S. Das Sarma, Rev. Mod. Phys. **80**, 1083 (2008).
[28] Particle-hole symmetry implies $u_{\bar{n},\bar{m}} = u^*_{n,m}$ and hence $u_{\gamma_j,\gamma_k} \in \mathbb{R}$.
[29] C. Hutter, A. Shnirman, Y. Makhlin, and G. Schön, Europhys. Lett. **74**, 1088 (2006).
[30] P. San-Jose, G. Zarand, A. Shnirman, and G. Schön, Phys. Rev. Lett. **97**, 076803 (2006).
[31] P. K. Tien and J. P. Gordon, Phys. Rev. **129**, 647 (1963).
[32] V. Mourik *et al.*, Science **336**, 1003 (2012).
[33] D. Rainis and D. Loss, Phys. Rev. B **85**, 174533 (2012).
[34] This term is similar to the nonadiabatic energy splitting which is shown in Sec. IV to decay exponentially with the distance between the Majorana modes.
[35] J. Klinovaja and D. Loss, Phys. Rev. B **86**, 085408 (2012).
[36] J. D. Sau, S. Tewari, and S. Das Sarma, Phys. Rev. A **82**, 052322 (2010).
[37] M. Freedman, C. Nayak, and K. Walker, Phys. Rev. B **73**, 245307 (2006).
[38] M. V. Berry, Proc. R. Soc. London, Ser. A. **414**, 31 (1987).
[39] S. Bravyi and A. Kitaev, Phys. Rev. A **71**, 022316 (2005).
[40] A. Romito, J. Alicea, G. Refael, and F. von Oppen, Phys. Rev. B **85**, 020502 (2012).
[41] T. Karzig, G. Refael, and F. von Oppen, arXiv:1305.3626.